



# CHORUS

This is the accepted manuscript made available via CHORUS. The article has been published as:

## Experimental study of the low-lying negative-parity states in $^{11}\text{Be}$ using the $^{12}\text{B}(d, ^3\text{He})^{11}\text{Be}$ reaction

J. Chen, K. Auranen, M. L. Avila, B. B. Back, M. A. Caprio, C. R. Hoffman, D. Gorelov, B. P. Kay, S. A. Kuvin, Q. Liu, J. L. Lou, A. O. Macchiavelli, D. G. McNeel, T. L. Tang, D. Santiago-Gonzalez, R. Talwar, J. Wu, G. Wilson, R. B. Wiringa, Y. L. Ye, C. X. Yuan, and H. L. Zang  
Phys. Rev. C **100**, 064314 — Published 20 December 2019

DOI: [10.1103/PhysRevC.100.064314](https://doi.org/10.1103/PhysRevC.100.064314)

# Experimental study of the low-lying negative-parity states in $^{11}\text{Be}$ using the $^{12}\text{B}(d, ^3\text{He})^{11}\text{Be}$ reaction

J. Chen,<sup>1,\*</sup> K. Auranen,<sup>1</sup> M. L. Avila,<sup>1</sup> B. B. Back,<sup>1</sup> M. A. Caprio,<sup>2</sup> C. R. Hoffman,<sup>1</sup> D. Gorelov,<sup>3,1</sup>  
B. P. Kay,<sup>1</sup> S. A. Kuvin,<sup>4</sup> Q. Liu,<sup>5</sup> J. L. Lou,<sup>5</sup> A. O. Macchiavelli,<sup>6</sup> D. G. McNeel,<sup>4</sup> T. L. Tang,<sup>1</sup>  
D. Santiago-Gonzalez,<sup>1</sup> R. Talwar,<sup>1</sup> J. Wu,<sup>1</sup> G. Wilson,<sup>7,1</sup> R. B. Wiringa,<sup>1</sup> Y. L. Ye,<sup>5</sup> C. X. Yuan,<sup>8</sup> and H. L. Zang<sup>5</sup>

<sup>1</sup>*Physics Division, Argonne National Laboratory, Argonne, Illinois 60439, USA*

<sup>2</sup>*Department of Physics, University of Notre Dame, Notre Dame, Indiana 46556, USA*

<sup>3</sup>*University of Manitoba, Department of Physics and Astronomy,  
Allen Building, Winnipeg, MB R3T 2N2, Canada*

<sup>4</sup>*Department of Physics, University of Connecticut, Storrs, Connecticut 06269, USA*

<sup>5</sup>*School of Physics and State Key Laboratory of Nuclear Physics and Technology, Peking University, Beijing 100871, China*

<sup>6</sup>*Nuclear Science Division, Lawrence Berkeley National Laboratory, Berkeley, California 94720, USA*

<sup>7</sup>*Department of Physics and Astronomy, Louisiana State University, Baton Rouge, Louisiana 70803, USA*

<sup>8</sup>*Sino-French Institute of Nuclear Engineering and Technology, Sun Yat-Sen University, Zhuhai 519082, China*

(Dated: November 20, 2019)

Low-lying negative-parity states in  $^{11}\text{Be}$  having dominant  $p$ -wave neutron configurations were studied using the  $^{12}\text{B}(d, ^3\text{He})^{11}\text{Be}$  proton-removal reaction in inverse kinematics. The  $1/2_1^-$  state at 0.32 MeV, the  $3/2_1^-$  state at 2.56 MeV and one or both of the states including the  $5/2_1^-$  level at 3.89 MeV and the  $3/2_2^-$  level at 3.96 MeV were populated in the present reaction. Spectroscopic factors were determined from the differential cross sections using a distorted wave Born approximation method. The  $p$ -wave proton removal strengths were well described by the shell model calculations while the Nilsson model calculation underestimates the spectroscopic factors for the higher excited states. Results from both Variational Monte Carlo and no-core shell model calculations were also compared with the experimental observations.

## I. INTRODUCTION

In light nuclei, the structure of the Be isotopes provides a great testing ground for numerous complementary nuclear models. The small number of valence nucleons allows for in-depth tests of the approximations made in single-particle calculations based on effective interactions in the shell model as well as more fundamentally based *ab-initio* calculations. In addition, the observation of structures with “deformation” properties in these isotopes opens an avenue for testing the validity of the Nilsson model or cluster model descriptions.

The duality of the collective and single-particle descriptions of the structure of the atomic nucleus has been probed by recent experimental work on  $^{18}\text{F}$  [1, 2] and the present system provides a similar testing ground for it. To further progress our understanding of the Be isotopes, we studied the proton-removal spectroscopic factors of the  $^{12}\text{B}(d, ^3\text{He})^{11}\text{Be}$  reaction and comparisons have been made with the effective-interaction shell model as well as the deformed Nilsson model. Further, the less model-dependent *ab-initio* calculations, which aspire to be able to predict rotational band structures in addition to single-particle features in light nuclei, were tested by their descriptions of  $^{11}\text{Be}$ , including the new data determined here.

The configurations of low-lying states in  $^{11}\text{Be}$  have been extensively studied, indicating quenching of  $N = 8$

shell gap and inversion of the  $0p$ - and  $1s0d$ -shells. While much attention has been paid to the  $1/2^+$  halo ground state, here we focus on the negative-parity states. The low-lying negative-parity states have been studied using the  $^9\text{Be}(t, p)^{11}\text{Be}$  reaction [3] and  $\beta$ -decay of  $^{11}\text{Li}$  [4–6]. These works interpreted the structure of the low-lying negative-parity states within the shell-model framework. The  $^9\text{Be}(^{13}\text{C}, ^{11}\text{C})^{11}\text{Be}$  reaction on the well-developed  $\alpha : n : \alpha$  structure of  $^9\text{Be}(\text{g.s.})$  populated the molecular structure of  $^{11}\text{Be}$  and suggested a rotational band  $K^\pi = 3/2^-$  built on the 3.96-MeV  $3/2_2^-$  state, which extends to the  $13/2^-$  state [7, 8]. Another band is believed to be headed with the relatively bound  $1/2_1^-$  state and terminated at the  $7/2^-$  state, which is currently the focus of this work. A summary of the previous studies on  $^{11}\text{Be}$  low-lying states can be found in Refs. [9, 10].

Studies on  $^{12}\text{B}$  have demonstrated the dominance of a  $0p$ -orbital neutron configuration in its ground state, which has a spin-parity of  $1^+$  [11–13]. With removal of one  $p$ -wave proton, the negative parity states in  $^{11}\text{Be}$  are able to be populated. The  $^{12}\text{B}(d, ^3\text{He})^{11}\text{Be}$  reaction can therefore be a probe of the neutron  $p$ -wave strength in  $^{11}\text{Be}$ . The present  $^{12}\text{B}(d, ^3\text{He})^{11}\text{Be}$  reaction solidifies the configuration of the low-lying negative-parity states and determines the strengths within the  $0p$ -shell orbitals. Negative-parity states with large  $\nu(2p-2h)$  configurations across the  $N = 8$  shell gap will not be strongly populated in this reaction, although allowed by the transferred angular momentum. An overall interpretation of the low-lying negative-parity states will be presented, which sheds light on the mixing between the  $1s0d$ - and the  $0p$ -shells as well as the structures of the  $0p$ -shell states in

\* chenjie@frib.msu.edu; Present address: National Superconducting Cyclotron Laboratory, East Lansing, Michigan 48824, USA

75  $^{11}\text{Be}$ .

## 76 II. EXPERIMENT

77 The  $^{12}\text{B}(d, ^3\text{He})^{11}\text{Be}$  reaction was carried out in inverse  
 78 kinematics at the ATLAS In-Flight Facility at Argonne  
 79 National Laboratory. The 12 MeV/u  $^{12}\text{B}$  secondary  
 80 beam was produced using the neutron adding reaction on  
 81 a  $^{11}\text{B}$  primary beam at 13.5 MeV/u. This beam, with an  
 82 intensity of 200 particle nano Amperes (pnA) bombarded  
 83 a 3.7-cm long  $\text{D}_2$  gas cell at a pressure of 1400 mbar and  
 84 temperature of 90 K. The resulting  $^{12}\text{B}$  was selected in  
 85 rigidity by the beam-line dipole magnets with a rate of  
 86 approximately  $2 \times 10^5$  particles per second and less than  
 87 5% contamination. The main contaminant,  $^7\text{Li}^{3+}$ , had  
 88 a much lower total energy than the  $^{12}\text{B}$  beam and was  
 89 easily separable in the analysis. Data from  $^{11}\text{B}(d, ^3\text{He})$   
 90 at 13.5 MeV/u was also collected at the beginning of the  
 91 experiment and served as an energy calibration and a  
 92 check of the analysis procedure.

93 The outgoing charged particles were analyzed by the  
 94 HELical Orbit Spectrometer (HELIOS) [14, 15] with a  
 95 magnetic field strength of 2.3 T and an experimental  
 96 setup resembling that shown in Fig. 2 of Ref. [16]. The  
 97  $^{12}\text{B}$  ions bombarded a deuterated polyethylene  $(\text{CD}_2)_n$   
 98 target of thickness  $400 \mu\text{g}/\text{cm}^2$  placed within the uniform  
 99 magnetic field at a position defined as  $Z = 0$  cm. The  $^3\text{He}$   
 100 particles from the reaction were transported through the  
 101 magnetic field to an array of 24 position-sensitive silicon  
 102 detectors (PSDs) that were positioned downstream of the  
 103 target covering a range of  $72 \text{ cm} < Z < 107 \text{ cm}$ . A group  
 104 of silicon  $\Delta E - E$  telescopes were placed at  $Z = 42$  cm to  
 105 identify the  $^9\text{-}^{11}\text{Be}$  reaction products. The thicknesses  
 106 of the  $\Delta E$  and  $E$  silicon detectors were  $\sim 75 \mu\text{m}$  and  
 107  $\sim 1000 \mu\text{m}$ , respectively.

108 The particle identification spectrum from the recoil  
 109 detectors for the  $^{12}\text{B}$  beam bombarding on the  $\text{CD}_2$   
 110 target appears in Fig. 1. The events in this figure  
 111 were selected by requiring a 150 ns timing coincidence  
 112 between a light particle detected in the HELIOS PSD  
 113 array and a recoil particle detected in the  $\Delta E - E$   
 114 telescope. The energy resolution was sufficient to identify  
 115 all of the Be isotopes of interest and thus discriminate  
 116 different reaction channels. The corresponding light  
 117 charged particles with each selected recoil were checked  
 118 by their cyclotron periods determined from the time  
 119 of flight information between the PSDs and  $\Delta E - E$   
 120 telescopes.

121 The  $^{11}\text{Be}$  in Fig. 1 were used to discriminate the  
 122  $^{12}\text{B}(d, ^3\text{He})^{11}\text{Be}$  transition to the bound state of  $^{11}\text{Be}$ . The  
 123  $^{10}\text{Be}$  ions, which have a much wider energy distribution,  
 124 were generated from the transition to the neutron-  
 125 unbound states of  $^{11}\text{Be}$ , which are above the neutron  
 126 separation energy ( $S_n = 0.502$  MeV) of  $^{11}\text{Be}$ . With the  
 127 energy loss of the escaping neutron, the average energy  
 128 of  $^{10}\text{Be}$  is lower than  $^{11}\text{Be}$ . Other possible sources of  
 129 the  $^{10}\text{Be}$  ions in Fig. 1, such as from the  $^{12}\text{B}(d, \alpha)^{10}\text{Be}$

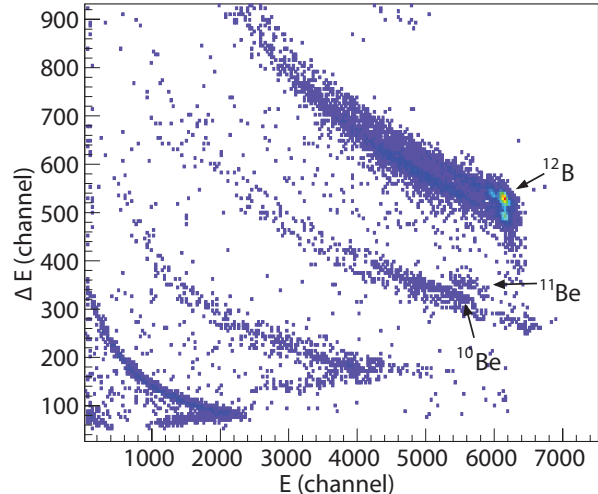


FIG. 1. The  $\Delta E - E$  spectrum obtained using one of the recoil detector telescopes with  $^{12}\text{B}$  incident on the  $(\text{CD}_2)_n$  target. The data shown required a coincidence with a particle in the PSD array. The particle groups labeled  $^{11}\text{Be}$  ( $^{10}\text{Be}$ ) and  $^{12}\text{B}$  are from neutron bound (unbound) states in  $^{11}\text{Be}$  and the elastic scattering of  $^{12}\text{B}$ , respectively.

130 reaction, were essentially excluded because the present  
 131 setup did not allow detection of the  $^{12}\text{B}(d, \alpha)$  reaction to  
 132 bound states of  $^{10}\text{Be}$ .

133 The incident beam flux was monitored by elastic  
 134 scattering events measured on the PSD array. The  
 135 elastic scattered deuterons on the beam particles were  
 136 selected by gating on a  $^{12}\text{B}$  ion identified in the recoil  
 137 detectors (see Fig. 1). The deuterons traveling for  
 138 four cyclotron periods were stopped on the PSDs and  
 139 their numbers were used to determine the integrated  
 140 number of incident particles times the target thickness,  
 141 the luminosity. Dividing the measured experimental  
 142 yield (which has been corrected for solid angle) by  
 143 the calculated elastic scattering cross sections gives the  
 144 luminosity of this measurement. The deuterons were  
 145 measured at an energy of  $\sim 3$  MeV and at a center of  
 146 mass (c.m.) angle of  $\sim 23^\circ$ , and their travelling periods  
 147 (four times their cyclotron period) were verified by the  
 148 time-of-flight information. A variety of optical model  
 149 potentials were used to calculate the elastic scattering  
 150 cross section. Uncertainties in the integral of the  $^{12}\text{B}$   
 151 beam particles times the target thickness varied with  
 152 an r.m.s of  $\sim 30\%$  depending on different optical model  
 153 parameters. A procedure for determining the absolute  
 154 yield is described in Section IV.

## 155 III. RESULTS

156 The light particles in the PSD array corresponding to  
 157 the  $^{12}\text{B}(d, ^3\text{He})^{11}\text{Be}$  reaction to the bound or unbound  
 158 states of  $^{11}\text{Be}$  were selected by a coincidence with  $^{11}\text{Be}$  or

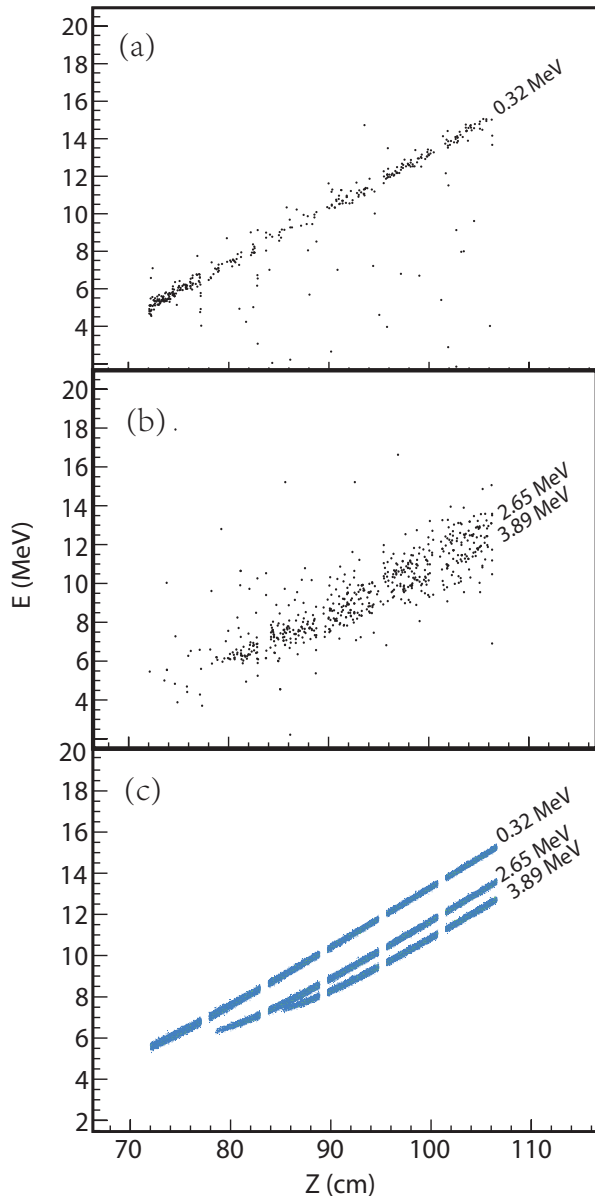


FIG. 2. Measured  ${}^3\text{He}$  energies ( $E$ ) as a function of the distance from the target ( $Z$ ) for the  ${}^{12}\text{B}(d,{}^3\text{He}){}^{11}\text{Be}$  reaction in inverse kinematics at 12 MeV/u with a magnetic field strength of 2.3 T. The data shown required a coincidence with either  ${}^{11}\text{Be}$  (a) or  ${}^{10}\text{Be}$  (b) recoils as shown in Fig. 1. Final states identified in  ${}^{11}\text{Be}$  are labelled by their corresponding excitation energies. (c) The simulation for the different excited states in the  ${}^{12}\text{B}(d,{}^3\text{He})$  reaction. See details in the text.

159  ${}^{10}\text{Be}$  ions discriminated in the recoil detectors (Fig. 1).  
 160 Most of the uncorrelated background was removed by  
 161 using this coincidence. The energies of the light particles  
 162 selected using this method are plotted in Fig. 2 versus the  
 163 corresponding distance where the particles were detected  
 164 by the PSD detectors.

165 For the present range covered by the PSD array, a

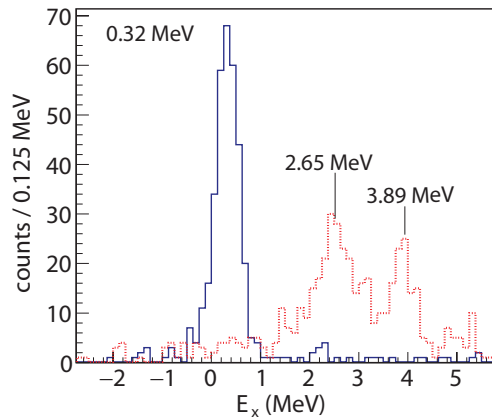


FIG. 3. The excitation-energy spectrum of  ${}^{11}\text{Be}$  neutron bound (blue solid line) and unbound (red dotted line) states determined from the data set presented in Fig. 2(a) and (b) respectively. States identified in the present work are labelled with their corresponding excitation energies.

166 clear isolated bound state in  ${}^{11}\text{Be}$  appears as a straight  
 167 line in the plot of Fig. 2a. For the unbound states,  
 168 their loci do not follow straight lines and different states  
 169 merge at around  $Z = 84$  cm. This is caused by the  
 170 shallow orbitals of the  ${}^3\text{He}$  particles which reached the  
 171 PSD detectors at radii of  $\sim 1.4$  cm at shorter distances  
 172 than the ideal situation. This effect was also observed  
 173 in the previous ( $d,{}^3\text{He}$ ) measurement [16]. It is also  
 174 seen in the Monte Carlo simulation of this reaction with  
 175 the present setup (see Fig. 2c). Events were selected  
 176 where the experimental kinematics loci are not merging  
 177 with each other, and were used to obtain the excitation  
 178 spectrum, as well as to evaluate the cross sections for the  
 179 unbound states. The events ( $Z < 85$  cm for the 2.65-  
 180 MeV state and  $Z < 90$  cm for the 3.89-MeV state) which  
 181 obviously deviate from the straight kinematics lines were  
 182 not used in the analysis.

183 Excitation spectra for the  ${}^{12}\text{B}(d,{}^3\text{He})$  reactions were  
 184 obtained from the projection of the data along the  
 185 kinematic lines and the results are shown in Fig. 3 for  
 186 both neutron-bound (blue) and unbound (red) states.  
 187 The resolution for the excitation-energy spectrum of the  
 188 bound state is around 560 keV (FWHM), dominated by  
 189 the properties of the beam and the energy loss and angle  
 190 straggling of  ${}^3\text{He}$  in the target. The measured widths  
 191 of the unbound states are also contributed to by their  
 192 intrinsic widths, which are 228(21) keV for the 2.65-MeV  
 193 state [3], 3.2(8) keV for the 3.89-MeV state [10] and 7.9(7)  
 194 keV for the 3.96-MeV states [10]. These widths are also  
 195 compatible with the present spectrum given the apparent  
 196 greater width of the 2.65-MeV state.

197 The peaks in Fig. 3 have been identified with the  
 198 states reported in the literature for  ${}^{11}\text{Be}$  [17] and are  
 199 listed in Table I. Below the neutron-separation energy  
 200 of  ${}^{11}\text{Be}$ , the  $1/2^-$  first-excited state at 0.32 MeV was  
 201 most strongly populated in the  ${}^{12}\text{B}(d,{}^3\text{He})$  reaction. The

TABLE I. Spectroscopic factors  $S$  extracted from the  $^{12}\text{B}(d,^3\text{He})^{11}\text{Be}$  reaction. The values are normalized such that the sum of  $S$  over all transitions is 3.0. Relative uncertainties on  $S$  are shown in parenthesis. Details on the uncertainties and the normalization factor are found in the text. Literature energies and spin-parity assignments are from Ref. [17].

Literature		Present data	
$E_x$ (MeV)	$J_\pi$	$l$	$S$
0.00 <sup>1</sup>	$1/2^+$		
0.32	$1/2^-$	$l = 1$	0.56(12)
1.78 <sup>1</sup>	$5/2^+$		
2.65	$3/2^-$	$l = 1$	1.49(44)
3.40 <sup>1</sup>	$3/2^{(+,-)}$		
3.89	$5/2^-$	$l = 1$	0.95(27)
3.96	$3/2^-$		
5.26 <sup>1</sup>	$5/2^-$		
6.71 <sup>1</sup>	$(7/2^-)$		

<sup>1</sup> Not observed in the present measurement. See details in the text.

202 unbound  $3/2_1^-$  state at 2.654 MeV also presents as a  
 203 strong transition in the present reaction. The next  
 204 peak, at 3.89 MeV, probably indicates population of  
 205 one or both of the states at 3.89 MeV and 3.96 MeV.  
 206 The relative contribution of these two states is discussed  
 207 in Section VI. The present resolution does not allow  
 208 separation of the ground state and first-excited state,  
 209 which are just 320 keV apart. A  $\chi^2$  fitting was carried  
 210 out assuming that both the ground state and the 0.32-  
 211 MeV state were populated. The best fit corresponded  
 212 to a population of the ground state at  $\sim 2\%$  of the  
 213 total events in the 0.32-MeV peak. We place an upper  
 214 limit on the population of the ground state at 10% of  
 215 the total events, based on the standard deviation of  $\chi^2$   
 216 method. Similarly, in Fig. 3, we cannot rule out some  
 217 population of the 3.410-MeV state, which was assigned as  
 218  $3/2^-$  or  $3/2^+$  in the previous study [3, 4, 18]. We place an  
 219 upper limit on the population of this state at 10% of the  
 220 total events populated in all combined unbound states.  
 221 The 5.26-MeV ( $5/2^-$ ) state is right at the edge of the  
 222 acceptance of the present setup, so no definite conclusion  
 223 for its population can be drawn here.

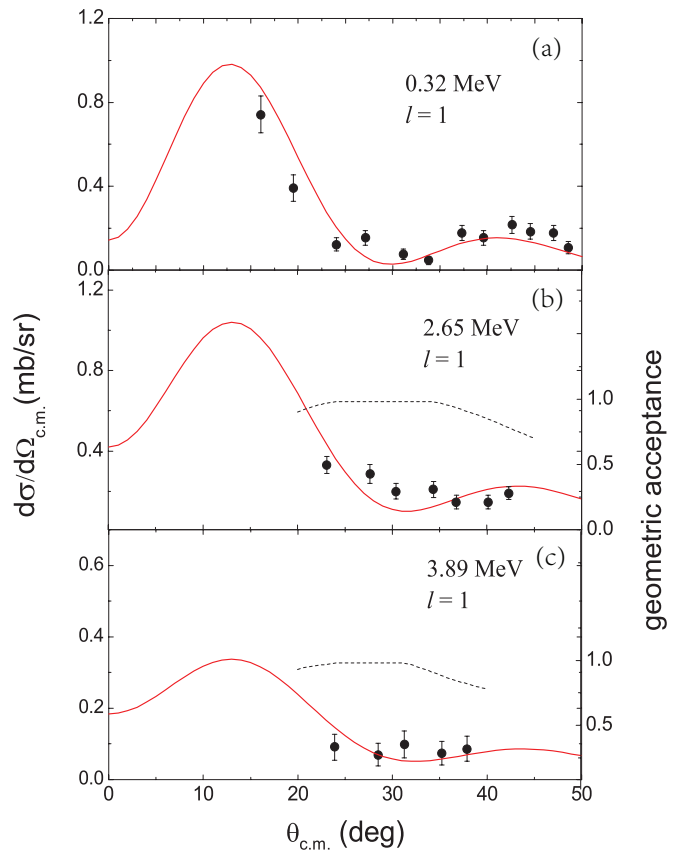


FIG. 4. Experimental (black points) and calculated (red solid lines) angular distributions for the (a) 0.32-, (b) 2.65- and (c) 3.89-MeV transitions in the  $^{12}\text{B}(d,^3\text{He})^{11}\text{Be}$  reaction. The curves represent DWBA calculations for  $l = 1$  transfer. Only statistical uncertainties are shown for the experimental data, and there is a systematic uncertainty of  $\sim 30\%$  on the absolute cross section scale. The geometrical acceptance of the  $^{10}\text{Be}$  recoils for the neutron-unbound states of  $^{11}\text{Be}$  is plotted as black dashed curves.

#### IV. ANGULAR DISTRIBUTIONS

225 The differential cross sections for each populated state  
 226 of the  $^{12}\text{B}(d,^3\text{He})^{11}\text{Be}$  reaction were deduced from the  
 227 present data using Eq. (4) in Ref. [19]. Every PSD  
 228 position was either considered as a single center-of-mass  
 229 angular bin or separated into two bins where the statistics  
 230 allowed. The center-of-mass angle ( $\theta_{cm}$ ) for each bin  
 231 was determined from the reaction kinematics and the  
 232 properties of HELIOS within an uncertainty of  $\sim 1^\circ$ . It  
 233 is noted that the acceptance of the recoiling  $^{10}\text{Be}$  generated  
 234 from the unbound states of  $^{11}\text{Be}$  might decrease due to  
 235 the breakup process compared to the acceptance of a  
 236 bound state. The geometrical acceptance of the  $^{10}\text{Be}$   
 237 ions, generated assuming isotropic decays of the  $^{11}\text{Be}$   
 238 unbound states, was calculated as a function of c.m.  
 239 angles and plotted in Fig. 4. Within the range of the

present data, the acceptance is mostly above 80% and it was used to correct the cross sections.

As stated in Section II, the total number of incident beam particles multiplied by the target thickness was estimated using the elastic scattering data measured on the PSD array. Combining this information, the solid angle coverage of the PSDs, and the counts of each state, absolute cross sections were obtained from the present analysis as shown in Fig. 4. Error bars in the figure are statistical only. There is a systematic uncertainty of around 30% for the absolute cross sections which includes the uncertainties from the determination of the integrated particle number and the cuts on the PID spectrum. Most of the discussions in this paper focus on the relative spectroscopic factor ( $S$ ), so the uncertainty in the absolute cross sections has very little impact on the conclusions that are drawn based on the present work.

## V. DWBA CALCULATIONS

The spectroscopic factors were extracted from the differential cross sections through a distorted wave Born approximation (DWBA) analysis calculated using the program PTOLEMY [20]. The optical model parameter sets of An *et al.* [21] and Pang *et al.* [22] were used as the entrance and exit channels. The Argonne  $v_{18}$  [23] potential was used to define the deuteron bound-state wave function and a Woods-Saxon potential with central potential well parameters of  $r_0 = 1.25$  fm and  $a_0 = 0.65$  fm, and with spin-orbit parameters of  $V_{so} = 6.0$  MeV,  $r_{so} = 1.1$  fm, and  $a_{so} = 0.65$  fm, was used to define the wave functions of the final proton bound states. The depth of the Woods-Saxon potential well was adjusted to reproduce the correct binding energy of each of the final proton bound states in  $^{11}\text{Be}$ .

The calculated cross sections were normalized to the experimental angular distributions of each populated state using a minimum  $\chi^2$  method. The results are presented in Fig. 4. For the 0.32-MeV state, the DWBA calculations with  $\ell = 1$  proton transfer reproduce the experimental angular distributions well. The 2.65-MeV and 3.89-MeV state data do not cover the most forward angular-distribution maximum due to the merged trajectories of these unbound states. Since the  $\ell = 1$  angular distribution of the 0.32-MeV state is well reproduced by the DWBA calculation, we fit the angular distributions of the 2.65-MeV and 3.89-MeV state for the experimental angular range, and larger uncertainties were determined for these states using various optical model potentials. The extracted spectroscopic factors  $S$  are listed in Table I, which have been normalized as described in Section VI. For the present reaction, the spectroscopic strengths are simply equivalent to the spectroscopic factors  $S$ .

A variety of optical model potentials [21, 22, 24–28] have been applied to the entrance and exit channels of the DWBA calculations to estimate uncertainties in

$S$ . For the relative  $S$ , the uncertainties arise from the statistics, the fitting procedure, and variations in the DWBA analysis, with the sum of them being  $\sim 10\%$  for the 320-keV state and  $\sim 20\%$  for the 2.65-MeV and 3.89-MeV states. Different reaction models may bring in an additional 10% uncertainty.

## VI. NORMALIZATION OF THE SPECTROSCOPIC STRENGTHS

In the present analysis, the observed  $p$ -wave strengths have been normalized to the expected occupancy of the two  $p$  orbitals using the Macfarlane and French sum rule [29]. In a simple single-particle picture, the sum of the observed strengths can be normalized to 3, the total number of protons expected to occupy the  $0p_{3/2}$  and  $0p_{1/2}$  orbitals in  $^{12}\text{B}$ . The 0.32-, 2.65- and 3.89-MeV states were all included in the normalization sum. The strengths from possible higher-lying negative-parity excited states, like the  $5/2^-$  state at 5.26 MeV, were assumed to be much smaller than those observed.

This assumption was supported by the shell model calculations discussed in Section VII A. This procedure results in a normalization factor of 0.73(26). The large uncertainty comes from the uncertainty in the absolute cross sections and the different optical model potentials.

The entire procedure for the extraction and normalization of the  $S$  values was checked using the  $^{11}\text{B}(d, ^3\text{He})$  data at 13.5 MeV/u taken with the same setup. We have obtained consistent normalized spectroscopic factors (see Section VII D) with those reported in Ref. [30] and using the same optical model parameters stated above.

## VII. DISCUSSION

In a shell-model picture, states of  $^{11}\text{Be}$  should only be strongly populated in the present reaction if doing so corresponds to removal of a  $p$ -shell proton from the ground state of  $^{12}\text{B}$ . The ground state of  $^{12}\text{B}$  is dominated by a  $p$ -shell neutron configuration, as shown by the neutron adding and proton removal reactions [12, 13, 31]. More specifically, one-proton removal reactions on  $^{13}\text{C}$  [11, 12, 32] indicate the  $^{12}\text{B}$  ground state is mostly in the  $\pi(0p_{3/2})^3\nu(0p_{1/2})^1$  configuration. Thus, states populated in the present reaction are expected to be dominated by a configuration of  $\pi(0p_{3/2})^2\nu(0p_{1/2})^1$ . Since a pair of protons in the  $0p_{3/2}$  orbital can couple to  $0^+$  or  $2^+$ , the full configuration can carry spin-parity values of  $J_\pi = 1/2^-, 3/2^-$  or  $5/2^-$ .

If we consider the low-lying structure of  $^{11}\text{Be}$  within the  $0p - 1s0d$  shells (which is reasonable since there is no indication for intruder of the  $1p0f$ -shell orbitals), negative-parity states in  $^{11}\text{Be}$  are predominantly comprised of two major neutron configurations, that is, the configuration within the  $0p$ -shell orbitals ( $0h\omega$ ), and

with two neutrons excited to the  $1s0d$ -shell ( $2\hbar\omega$ ). The present reaction should selectively populate states with a dominant  $0\hbar\omega$  configuration.

There are three major peaks that were strongly populated in this reaction, as shown in Fig. 3, corresponding to the  $1/2_1^-$  state at 0.32 MeV, the  $3/2_1^-$  state at 2.65 MeV, plus one or both of the  $5/2_1^-$  state at 3.89 MeV and the  $3/2_2^-$  state at 3.96 MeV. The  $1/2_1^-$  state at 0.32 MeV is expected, in a shell-model description, to be dominated by the normal  $p$ -shell neutron configuration. This was confirmed by the one-neutron transfer reaction  $^{10}\text{Be}(d,p)^{11}\text{Be}$  [33], which gives a large spectroscopic factor ( $S = 0.62(4)$ ) for the  $\ell = 1$  neutron component in this state. The  $3/2_1^-$  state at 2.65 MeV was previously seen in the  $(t,p)$  reaction [3] and  $\beta$ -decay of  $^{11}\text{Li}$  [4], suggesting a normal  $p$ -shell neutron configuration as well. Our result confirms these observations. The state at 3.889 MeV was previously assigned as  $3/2^+$  in the  $^9\text{Be}(t,p)^{11}\text{Be}$  reaction measurement [3]. However, the  $\beta$ -delayed decay study [4] revised the spin-parity of this state to  $5/2^-$ . Regarding the likely population of this state in the present measurement, our results are consistent with the  $5/2^-$  negative-parity assignment.

There are also some negative-parity states which previous experimental work have indicated to be dominated by configurations with two-neutrons excited into the  $sd$ -shell. The  $3/2_2^-$  state is suggested to be dominated by a configuration of  $^9\text{Be}\otimes(sd^2)_{(2^+)}$  experimentally (see Table I in Ref. [9]) as well as in the shell-model calculation (see Sec. VII A). The  $3/2_2^-$  state at 3.955 MeV should not be strongly populated in the present measurement if there is only a small amount of mixing between the  $3/2_1^-$  and  $3/2_2^-$  states. The situation is similar for the  $5/2_2^-$  state at 5.26 MeV.

In the following subsections, results with the effective-interaction shell model, Nilsson model, variational Monte Carlo (VMC), and no-core configuration interaction (NCCI) frameworks are compared with experiment. Some of these results are also summarized in Table II and Fig. 5.

### A. Shell model calculations

We have performed shell model calculations for  $^{12}\text{B}$  and  $^{11}\text{Be}$  with the recently developed YSOX interaction [34] using the OXBASH code [36]. The calculations assumed  $^4\text{He}$  as an inert core, and particles could occupy the  $0p_{1/2}$ ,  $0p_{3/2}$ ,  $1s_{1/2}$ ,  $0d_{5/2}$  and  $0d_{3/2}$  orbitals. The calculated  $^{11}\text{Be}$  excitation energies and corresponding spectroscopic factors are given in Table II as well as Fig. 5. Further information about the occupation number of each orbital can be found in Table III. The YSOX interaction reproduces well the ground-state energies, energy levels, electric quadrupole properties, and spin properties for most nuclei in the full  $psd$  model space including  $(0 - 3)\hbar\omega$  excitations [34].

Comparison is also made with calculations using the WBP interaction [37]. While the WBP interaction gives the lowest  $1/2^-$  and  $1/2^+$  states in “normal” order, the YSOX interaction reproduces the experimentally-observed parity inversion, albeit with a larger splitting (0.90 MeV) than observed experimentally (0.32 MeV). We will therefore focus on the calculations with the YSOX interaction in the following discussion.

According to the calculations using the YSOX interaction, the spectroscopic factors to all positive parity states can be neglected ( $S < 0.01$ ) in the  $^{12}\text{B}(d,^3\text{He})^{11}\text{Be}$  reaction. The  $1/2_1^-$ ,  $3/2_1^-$  and  $5/2_1^-$  states have large overlaps with the  $^{12}\text{B}$  g.s., corresponding to the experimentally observed states at 320 keV, 2.654 MeV, and 3.899 MeV. These states have a configuration with one particle in the  $0p_{1/2}$  orbital and with very little excitation to the  $sd$ -shell, consistent with our previous discussion. The calculated  $S$  (Table II) of the former two states are in reasonable agreement with the experimental values. The  $3/2_2^-$  state in the calculation probably corresponds to the 3.96-MeV state, and it is dominated by a  $2\hbar\omega$  configuration, which has a smaller overlap with the  $^{12}\text{B}$  g.s. The  $S$  of the  $3/2_2^-$  and the  $5/2_1^-$  state are added and compared with the experimental spectroscopic factor of the doublet around 3.89 MeV, showing reasonable agreement. If we assume small mixing between the  $3/2_1^-$  and  $3/2_2^-$  states, the experimentally observed events at around 3.89 MeV should be dominated by the 3.89-MeV  $5/2^-$  state, with only a small contribution from the 3.96-MeV  $3/2_2^-$  state due to the configuration mixing of the  $0\hbar\omega$  excitation.

The maximum angular momentum that can be obtained within the  $p$ -shell orbitals is  $7/2^-$ . With a transferred angular momentum of  $\ell = 1$ , the present reaction cannot populate states of this angular momentum. Nonetheless, we list the shell-model calculations for the first two  $7/2^-$  states in Tables II and III for comparison. There is no firmly-assigned experimental  $7/2^-$  state in the literature [17].

There is a  $5/2_2^-$  state at around 6 MeV in the calculation with a  $2\hbar\omega$  configuration which could naturally be identified with the previously observed 5.255-MeV state in the  $^9\text{Be}(t,p)$  reaction [3]. This state could not be observed in the present measurement due to the acceptance of the setup. However, the calculated spectroscopic factor for this state is much smaller than the  $5/2_1^-$  state or the  $3/2_1^-$  states, indicating the  $p$ -wave strength observed in this measurement could account for most of the proton removal strengths. This suggests that it is reasonable to normalize the sum of them to the occupancy of the  $p$ -wave orbital in the  $^{12}\text{B}$  g.s., as done in Sec. VI.

### B. Nilsson model calculations

The strong  $\alpha$  clustering in  $^8\text{Be}$  naturally suggests that deformation degrees of freedom will play an important

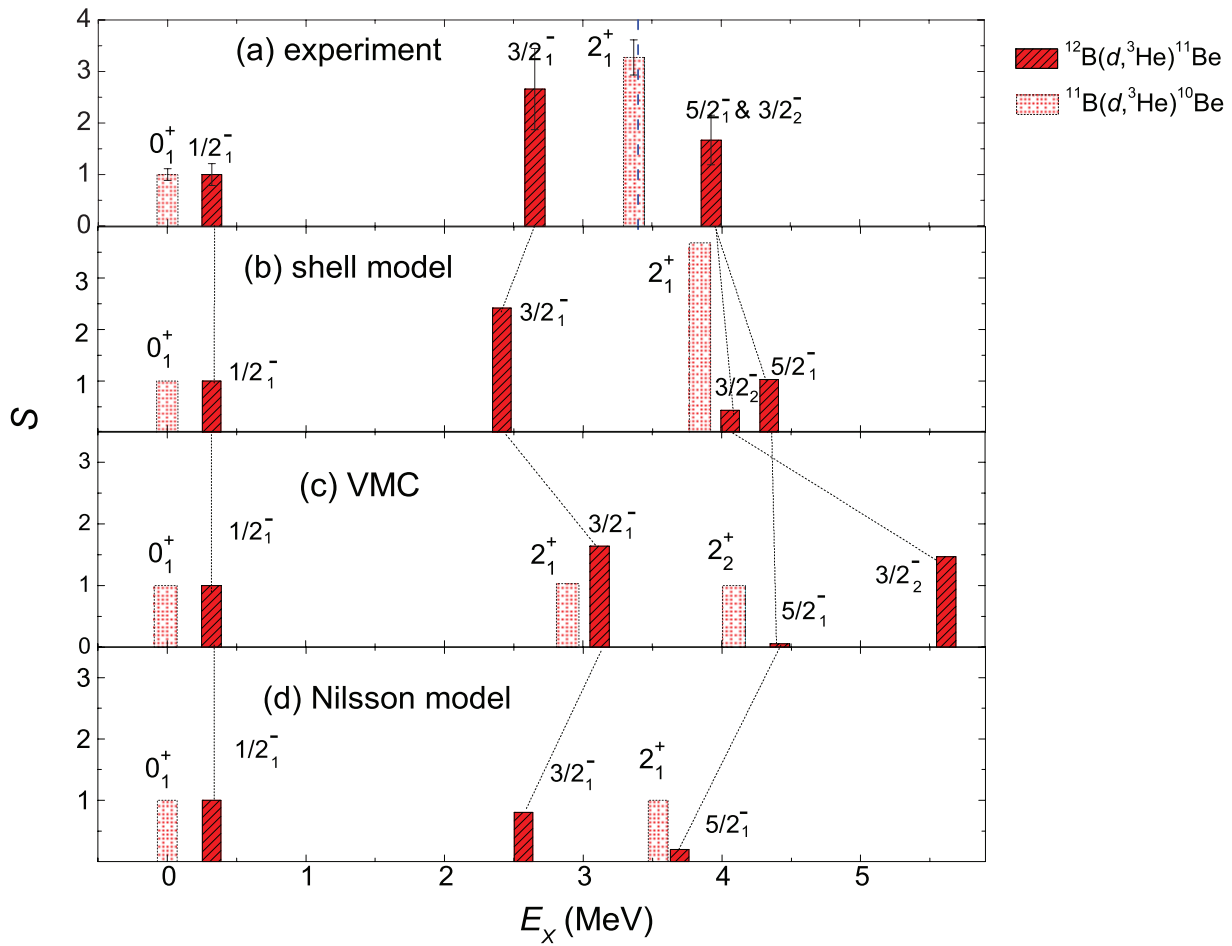


FIG. 5. The experimental (a) and calculated (b,c,d) excitation energies and spectroscopic factors of the  $1/2_1^-$ ,  $3/2_1^-$ ,  $5/2_1^-$  states of  $^{11}\text{Be}$  from the  $^{12}\text{B}(d,^3\text{He})^{11}\text{Be}$  reaction (slash bars) and  $0_1^+$  and  $2_1^+$  states of  $^{10}\text{Be}$  from the  $^{11}\text{B}(d,^3\text{He})^{10}\text{Be}$  reaction (dotted bars). Results shown in panels (b), (c) and (d) were calculated using the shell model with YSOX interaction [34], the VMC method [23], and the Nilsson model [35], respectively. The error bars for the experimental values are just for relative  $S$ . The blue dashed line in (a) is the  $(2j+1)$ -weighted energy centroid of  $3/2_1^-$  and  $5/2_1^-$  states in  $^{11}\text{Be}$ . Note that the spectroscopic factors and excitation energies of the first excited state in (a, b, c, d) were normalized to unity and the experimental value ( $E_x = 0.32$  MeV), respectively.

456 role on the structure of the Be isotopes, a topic that  
 457 has been extensively discussed in the literature (see [38]  
 458 for a review). The deformation in  $^8\text{Be}$  is evidenced by  
 459 the ground state rotational band and the enhanced E2  
 460 transition [39]. Furthermore, Bohr and Mottelson [40]  
 461 proposed the effects of deformation to explain the  
 462 inversion of the  $1/2^+$  and the  $1/2^-$  states.

463 Here we attempt to describe the spectroscopic factors  
 464 data in terms of the Nilsson model in the strong coupling  
 465 limit. Within this framework, the  $K = 1/2^-$  can  
 466 be associated with the neutron  $1/2[220]$  level. The  
 467 excitation energies follow

$$E_x(J) = E_0 + \frac{\hbar^2}{2\Theta} [J(J+1) + a(-)^{J+1/2}(J+1/2)], \quad (1)$$

468 with the rotational parameter  $b = \hbar/2\Theta = 0.5$  MeV

469 and a decoupling parameter  $a = 0.5$  in line with Nilsson  
 470 calculations for deformations of  $0.3-0.4$ . This band is  
 471 expected to be terminated by the  $7/2^-$  state with all the  
 472 angular momentum of the valence nucleons aligned. It  
 473 appears that the second  $7/2^-$  state in Table II and III  
 474 belongs to this band due to its dominant configuration  
 475 within the  $p$ -shell.

476 For  $Z = 5$ , the last proton is expected to occupy  
 477 the  $3/2[101]$  level and the g.s. of  $^{12}\text{B}$  is the bandhead  
 478 of the  $K = 1$  band originating from the coupling of  
 479 the two Nilsson levels above. Since the level parentage  
 480 is attributed only to the  $0p_{3/2}$  orbit, the spectroscopic  
 481 factors depend only on the Clebsch-Gordan coefficients  
 482 according to Eq. 3 of Ref. [35], and we predict the  $S$  as  
 483 listed in Table II and shown in Fig. 5. The spectroscopic  
 484 factors of the  $3/2_1^-$  and  $5/2_1^-$  states were underestimated

TABLE II. Excitation energies  $E_x$  and spectroscopic factors  $S$  for the  $^{12}\text{B}(d,^3\text{He})^{11}\text{Be}$  reaction calculated by the shell model using the YSOX [34] interaction, the Nilsson model [35], and the VMC calculations with the AV18+UX potential [23]. Each set of  $S$  values have been normalized to the first excited state ( $1/2_1^-$ ) state with normalization factors 0.521, 0.5, 0.274 and 0.56(12) of for the YOSX interaction, the Nilsson model, the VMC calculation and the experiment, respectively.. The VMC  $E_x$  are set relative to the experimental  $1/2^+$  energy and the numbers in parentheses are the Monte Carlo error in the last digit. Also see Fig. 5.

$^{11}\text{Be}$ $J_\pi$	YSOX		Nilsson		VMC		Experiment	
	$E_x$ (MeV)	$S$	$E_x$ (MeV)	$S$	$E_x$ (MeV)	$S$	$E_x$ (MeV)	$S$
$1/2_1^+$	0.00	0.003					0.00	
$1/2_1^-$	0.897	1.00	0.125	1.00	0.3(2)	1.00	0.32	1.00(21)
$5/2_1^+$	1.355	0.004					1.78	
$3/2_1^-$	3.091	2.416	2.375	0.8	3.1(4)	1.64	2.65	2.66(79)
$3/2_1^+$	3.994	< 0.001					3.41	
$5/2_1^-$	4.918	1.033	3.569	0.2	4.4(4)	0.06	3.89	1.67(48)
$3/2_2^-$	4.636	0.432			5.6(4)	1.47	3.96	
$5/2_2^-$	6.105	< 0.001			9.4(4)	0.38	5.26	
$7/2_1^-$	6.671	< 0.001			11.2(4)		(6.71)	
$7/2_2^-$	9.365	< 0.001	8.875	0.0				

TABLE III. Shell-model occupation numbers for  $^{12}\text{B}$  and  $^{11}\text{Be}$  with the YSOX interaction.

Nuclide	$J_\pi$	$E_x$ (MeV)	Protons					Neutrons				
			$0p_{3/2}$	$0p_{1/2}$	$0d_{5/2}$	$0d_{3/2}$	$0s_{1/2}$	$0p_{3/2}$	$0p_{1/2}$	$0d_{5/2}$	$0d_{3/2}$	$0s_{1/2}$
$^{12}\text{B}$	$1^+$	0.000	2.701	0.193	0.04	0.052	0.014	3.733	1.117	0.071	0.061	0.018
$^{11}\text{Be}$	$1/2_1^+$	0.000	1.747	0.222	0.009	0.017	0.005	3.459	0.483	0.227	0.04	0.792
	$1/2_1^-$	0.897	1.8	0.162	0.009	0.025	0.005	3.85	1.05	0.05	0.042	0.009
	$5/2_1^+$	1.355	1.71	0.259	0.01	0.017	0.004	3.442	0.502	0.859	0.061	0.137
	$3/2_1^-$	3.091	1.797	0.148	0.015	0.03	0.009	3.374	1.138	0.294	0.061	0.133
	$3/2_1^+$	3.994	1.697	0.269	0.012	0.018	0.005	3.388	0.552	0.244	0.208	0.608
	$3/2_2^-$	4.636	1.658	0.314	0.01	0.015	0.004	2.935	0.545	0.718	0.125	0.677
	$5/2_1^-$	4.918	1.769	0.179	0.019	0.026	0.007	3.788	1.027	0.095	0.055	0.035
	$5/2_2^-$	6.105	1.624	0.356	0.006	0.011	0.003	2.675	0.41	1.032	0.176	0.792
	$7/2_1^-$	6.671	1.629	0.343	0.008	0.016	0.004	2.614	0.418	1.145	0.233	0.59
$7/2_2^-$	9.365	1.884	0.041	0.029	0.036	0.01	2.919	1.693	0.063	0.239	0.086	

in this framework, perhaps suggesting deviations (due to Coriolis coupling) from the strong coupling limit for the odd-odd  $^{12}\text{B}$   $K = 1$  band that should be explored.

directly to our understanding of the inter-nucleon interactions [23, 51, 52]. In the following, we present two sets of *ab initio* calculations that use realistic interactions fit to  $NN$  elastic scattering data: variational Monte Carlo (VMC) and no-core configuration interaction (NCCI).

### C. *Ab-initio* theory

*Ab-initio* nuclear theory sets out to predict nuclear properties starting directly from the description of the nucleus as a system of interacting nucleons [41–50]. The aim is to provide a predictive theory which removes the simplifying assumptions of phenomenological approaches and ties the predictions for the many-body system

#### 1. Variational Monte Carlo calculations

The VMC calculations begin with the construction of correlated wave functions  $\Psi(J^\pi, T, T_z)$  for the nuclei of interest as approximate solutions of the nonrelativistic Schrödinger equation  $H\Psi = E\Psi$ . In the present work we

505 use the Argonne  $v_{18}$  two-nucleon and Urbana X three-  
 506 nucleon potentials (AV18+UX) for our Hamiltonian.  
 507 The wave functions are constructed from products of  
 508 two- and three-body correlation operators acting on an  
 509 antisymmetric single-particle state of the appropriate  
 510 quantum numbers. The correlation operators are  
 511 designed to reflect the influence of the two- and three-  
 512 nucleon potentials at short distances, while appropriate  
 513 boundary conditions are imposed at long range. The  
 514  $\Psi(J^\pi, T, T_z)$  have embedded variational parameters that  
 515 are adjusted to minimize the energy expectation value,

$$E_V = \frac{\langle \Psi | H | \Psi \rangle}{\langle \Psi | \Psi \rangle} \geq E_0, \quad (2)$$

516 which is evaluated by Metropolis Monte Carlo in-  
 517 tegration. The VMC wave functions serve as the  
 518 starting point for exact Green's function Monte Carlo  
 519 (GFMC) calculations, which have been very successful  
 520 in reproducing energies, electromagnetic moments and  
 521 transition rates, in light nuclei up to  $^{12}\text{C}$ . However,  
 522 GFMC calculations have not yet been made for the  $^{11}\text{Be}$   
 523 and  $^{12}\text{B}$  nuclei studied here. A comprehensive review of  
 524 the VMC and GFMC methods is given in Ref. [50].

525 For the negative parity states in  $^{11}\text{Be}$  the single-  
 526 particle state is constructed in  $LS$  coupling with all  
 527 possible [4421] and [4331] spatial symmetries within the  
 528 p-shell, as specified in Young diagram notation, including  
 529 2P, 2D, 2F[4421] and 2S, 4S, 2D, 4D[4421] components.  
 530 The relative strengths of these components are obtained  
 531 in a small-basis diagonalization after all the correlations  
 532 have been applied. The first six negative-parity states  
 533 are  $1/2^-$ ,  $3/2^-$ ,  $5/2^-$ ,  $3/2^-$ ,  $5/2^-$ , and  $7/2^-$ , as shown  
 534 in Table II, in agreement with the observed experimental  
 535 ordering, although with a greater spread in excitation  
 536 energies. The unnatural parity  $1/2^+$  ground state has  
 537 not yet been evaluated, so the excitation energies shown  
 538 assume a 0.3 MeV starting point for the  $1/2^-$  state.

539 The low-lying states in  $^{12}\text{B}$  are constructed starting  
 540 from single-particle states with all possible [4431]  
 541 spatial symmetries within the p-shell, including 3P,  
 542 3D, 3F, 1P, and 1D components. After the small-  
 543 basis diagonalization, we find considerable degeneracy  
 544 amongst the low-lying states, with two  $1^+$  and a  $2^+$   
 545 levels all in close proximity. While this is not an entirely  
 546 satisfactory status, for the present purpose we identify  
 547 the  $1^+$  state that has positive magnetic and quadrupole  
 548 moments as the ground state, and use it to evaluate the  
 549 spectroscopic overlaps with  $^{11}\text{Be}$ , following the method  
 550 discussed in Ref. [53]. The absolute spectroscopic  
 551 factors obtained are significantly quenched relative to the  
 552 nominal occupation of 3 protons in  $^{12}\text{B}$ , but the relative  
 553 spectroscopic factors given in Table II and Fig. 5 are  
 554 normalized to the first excited state ( $1/2_1^-$ ) as for the  
 555 other calculations.

556 Compared to the experimental values, the VMC  
 557 calculation presents a correct level order for the low-lying  
 558 negative-parity states, but the energy difference of the  
 559  $3/2_2^-$  and  $5/2_1^-$  is much larger than the experimental

560 values. The calculated spectroscopic factors show a  
 561 reasonable agreement with the experiment. Compared  
 562 to the shell model calculation, the spectroscopic factor  
 563 of the  $3/2_2^-$  state is much larger than the  $5/2_1^-$  state,  
 564 indicating larger mixing of the  $0\hbar\omega$  and  $2\hbar\omega$  configuration  
 565 in this calculation.

## 566 2. No-core configuration interaction calculations

567 Here we examine the extent to which *ab-initio*  
 568 NCCI calculations predict a low-lying spectrum for  
 569  $^{11}\text{Be}$  consistent with that experimentally observed in  
 570  $^{11}\text{Be}$ . We focus on the negative-parity states, and use  
 571 the Daejeon16 nucleon-nucleon interaction [54]. These  
 572 calculations, presented in further detail in Refs. [55], are  
 573 carried out with the NCCI code MFDn [56–58].

574 In the no-core configuration interaction (NCCI), or  
 575 no-core shell model (NCSM), approach [48], the many-  
 576 body Schrödinger equation is solved in a basis of Slater  
 577 determinants (antisymmetrized products) of harmonic  
 578 oscillator orbitals. In practice, this basis must be  
 579 truncated, generally at some maximum number  $N_{\text{max}}$  of  
 580 oscillator excitations. The results converge, a  $N_{\text{max}} \rightarrow$   
 581  $\infty$ , towards the solution to the original, untruncated  
 582 Schrödinger equation problem. The accuracy of  
 583 this solution is constrained by available computational  
 584 resources and thus maximum accessible  $N_{\text{max}}$  for the  
 585 basis. We must verify that any calculation at finite  
 586  $N_{\text{max}}$  yields sufficiently accurate (or converged) results  
 587 to permit meaningful comparison of observables with  
 588 experiment (*e.g.*, Refs. [59–62]).

589 The low-lying negative parity spectrum for  $^{11}\text{Be}$ ,  
 590 calculated with a basis truncation of  $N_{\text{max}} = 10$  (and  
 591 a basis oscillator parameter of  $\hbar\omega = 15$  MeV), is  
 592 shown in Fig. 6(a). Although the absolute (or binding)  
 593 energies are not well-converged in the calculation (they  
 594 change by an MeV or more between the  $N_{\text{max}} = 8$   
 595 and 10 calculations), many of the features of the low-  
 596 lying *excitation* spectrum, or *relative* energies between  
 597 states, are in fact much more robustly converged in the  
 598 calculations. In general, the low-lying rotational band  
 599 structure emerges at comparatively low  $N_{\text{max}}$  in NCCI  
 600 calculations of the Be isotopes [55, 63–65]. Rotational  
 601 energy fits to the lowest negative parity band ( $K^P =$   
 602  $1/2^-$ ) and excited negative parity band ( $K^P = 3/2^-$ )  
 603 are shown in Fig. 6(a).

604 The relative energies of the members of the lowest  
 605 negative parity band, from the NCCI calculations, are  
 606 shown in Fig. 6(b). The calculated relative energies  
 607 within the  $K^P = 1/2^-$  band are comparatively  
 608 independent of  $N_{\text{max}}$ , varying by less than  $\sim 0.1$  MeV,  
 609 at  $N_{\text{max}} = 10$ . Comparing with experiment [dashes in  
 610 Fig. 6(b)], the NCCI prediction for the relative energy  
 611 of the  $3/2^-$  and  $1/2^-$  band members is consistent with  
 612 experiment to within  $\sim 0.1$  MeV. The  $5/2^-$  assignment  
 613 for the state at 3.89 MeV places the *ab initio* calculated  
 614 and experimental values for the relative energy of the

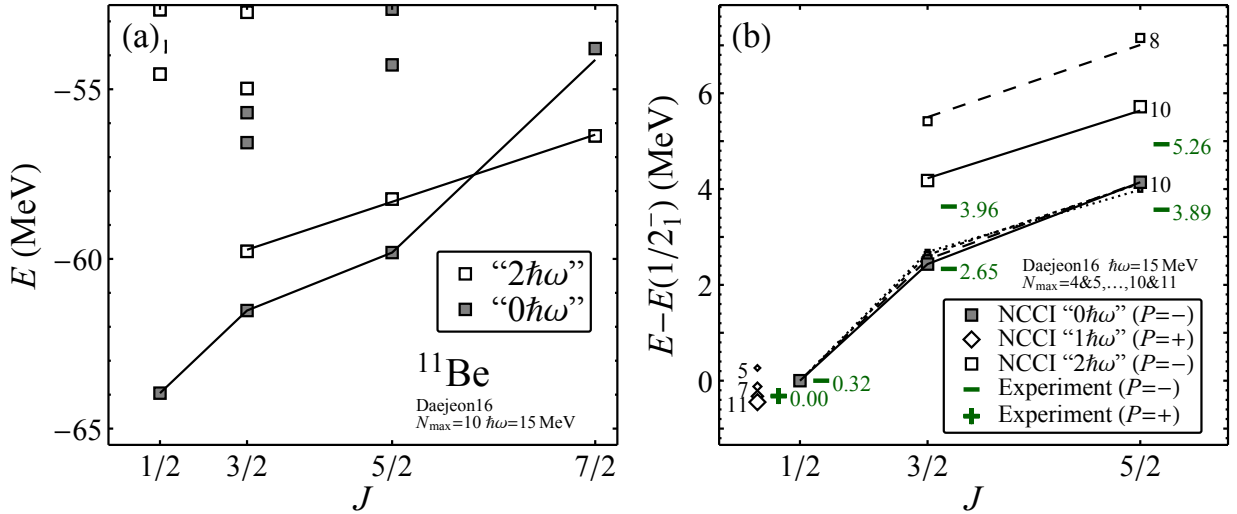


FIG. 6. *Ab initio* NCCI calculated energy spectrum for negative parity states of  $^{11}\text{Be}$  with the Daejeon16 interaction. Energies are plotted against an angular momentum axis scaled as  $J(J+1)$ , as appropriate for rotational analysis. (a) Calculated negative parity spectrum ( $N_{\text{max}} = 10$ ,  $\hbar\omega = 15$  MeV), shown with fits of the rotational energy formula (1) to the calculated band member energies (lines). States are classified as “ $0\hbar\omega$ ” (shaded square) or “ $2\hbar\omega$ ” (open squares) as described in the text. (b) Calculated *relative* energies, taken with respect to the  $1/2_1^-$  “ground state” of the negative parity space. These are shown for successively larger bases, as indicated by increasing symbol size, from  $N_{\text{max}} = 4$  (dotted line) through 10 (solid line). The relative energy of the calculated  $1/2_1^+$  is also shown (diamonds), from  $N_{\text{max}} = 5$  through 11. Energies for the experimental counterparts are shown (“-” for negative parity or “+” for positive parity) for comparison (these are labeled with the experimental excitation energies, in MeV, for convenient identification).

615  $3/2^-$  and  $1/2^-$  band members in agreement to within  
616  $\sim 0.6$  MeV.

617 To place these negative parity states in the context  
618 of the positive parity ground state, we also show  
619 the energy of the  $1/2_1^+$  state relative to the  $1/2_1^-$  in  
620 Fig. 6(b). While this energy difference is not quite  
621 as well-converged with  $N_{\text{max}}$  as those between the  
622 negative-parity band members, it is already apparent  
623 that the Daejeon16 interaction reproduces (and, in fact,  
624 somewhat overestimates) the experimentally observed  
625 parity inversion [66, 67].

626 However, the calculated excitation energy of the  
627 excited  $K^P = 3/2^-$  band, relative to the  $1/2_1^-$   
628 state, is still highly sensitive to the basis truncation.  
629 While the calculated energies are decreasing towards the  
630 experimental values with increasing  $N_{\text{max}}$  [Fig. 6(b)], it is  
631 not yet possible to reliably estimate what the converged  
632 values might be and to make a meaningful comparison.

633 At a qualitative level, the low-lying states obtained in  
634 the present NCCI calculation for  $^{11}\text{Be}$  may be classified  
635 into “ $0\hbar\omega$ ” and “ $2\hbar\omega$ ” states, as indicated in Fig. 6(a)  
636 (by the shaded and open symbols, respectively), based  
637 on their calculated wave functions. Taking the  $5/2_1^-$  and  
638  $5/2_2^-$  states for illustration, in Fig. 7, we examine the  
639 contributions to the norm (or probability) coming from  
640 oscillator configurations with  $N_{\text{ex}} = 0, 2, 4, \dots$  excitation  
641 quanta relative to the lowest permitted filling of oscillator  
642 shells, *i.e.*, the  $0\hbar\omega$ ,  $2\hbar\omega$ , *etc.*, components of the wave

643 function. For the  $5/2_1^-$  state [Fig. 7(b)], the contribution  
644 from  $0\hbar\omega$  oscillator configurations dominates (although  
645 some of this probability bleeds off to higher  $N_{\text{ex}}$   
646 contributions as  $N_{\text{max}}$  increases). In contrast, for the  
647  $5/2_2^-$  state [Fig. 7(a)], the  $0\hbar\omega$  contribution is highly  
648 suppressed, with the largest contribution coming from  
649  $2\hbar\omega$  and then falling off gradually for higher  $N_{\text{ex}}$ . In this  
650 sense, the NCCI calculations suggest a “ $0\hbar\omega$ ” character  
651 for the  $K^P = 1/2^-$  band members ( $1/2_1^-$ ,  $3/2_1^-$ ,  $5/2_1^-$ ,  
652  $\dots$ ) and a “ $2\hbar\omega$ ” character for the  $K^P = 3/2^-$  band  
653 members ( $3/2_2^-$ ,  $5/2_2^-$ ,  $\dots$ ).

#### 654 D. Comparisons with $^{11}\text{B}(d,^3\text{He})^{10}\text{Be}$ data

655 The  $^{11}\text{B}(d,^3\text{He})^{10}\text{Be}$  reaction also serves as a testing  
656 ground for the different theoretical models. Information  
657 could be obtained from previous data as well as the  
658 stable beam data in the present experiment. The present  
659 measurement gives spectroscopic factors of 0.61(6),  
660 2.09(21) and 0.30(6) for the g.s. ( $0^+$ ),  $2_1^+$  and  $2_2^+$  state,  
661 which is consistent with the previous measurement [30].  
662 In order to further understand the experimental results,  
663 we also compare the experimental spectroscopic factors  
664 of the  $^{11}\text{B}(d,^3\text{He})^{10}\text{Be}$  reaction to the calculated ones of  
665 the shell model using the YSOX interaction, the Nilsson  
666 model, and the VMC calculation. Fig. 5 represents these

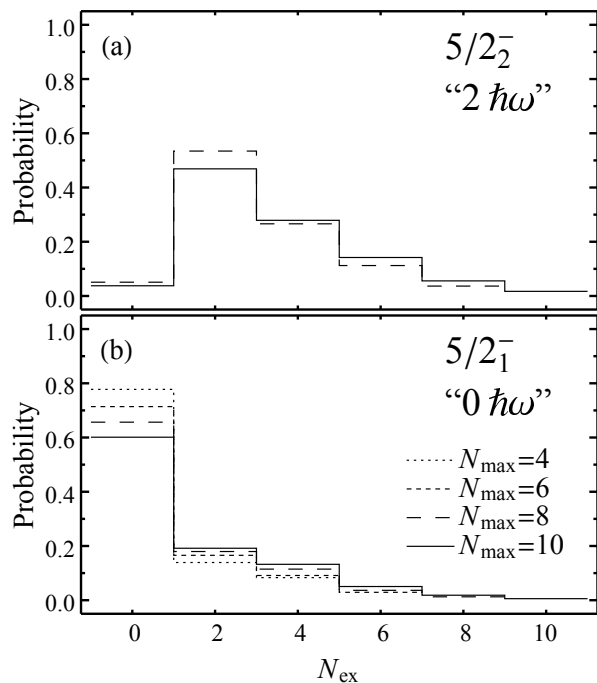


FIG. 7. Decomposition of NCCI calculated eigenstates for the (a)  $5/2_2^-$  and (b)  $5/2_1^-$  states, with respect to the number of excitation quanta  $N_{\text{ex}}$  in the contributing oscillator configurations. These decompositions are for the same calculations as shown in Fig. 6(b), with the histograms overlaid for  $N_{\text{max}} = 4$  (dotted line) through 10 (solid line).

667 calculated spectroscopic factors and excitation energies  
 668 in comparison with the experiments for the  $1/2_1^-$ ,  $3/2_1^-$ ,  
 669  $5/2_1^-$  states of  $^{11}\text{Be}$  in the  $^{12}\text{B}(d, ^3\text{He})^{11}\text{Be}$  reaction and  
 670  $0_1^+$  and  $2_1^+$  states of  $^{10}\text{Be}$  in the  $^{11}\text{B}(d, ^3\text{He})^{10}\text{Be}$  reaction.  
 671 The excitation energy of the  $2^+$  state of  $^{10}\text{Be}$  in the  
 672 Nilsson model was calculated using  $b = 0.59$ . It is  
 673 noted that the calculated excitation energies of the  $1/2^-$   
 674 state were all normalized to the experimental value and  
 675 its spectroscopic factors were normalized to unity in  
 676 order to compare the relative excitation energies and  
 677 spectroscopic factors of the negative-parity states in these  
 678 different calculations on equal footing.

679 Experimental and theoretical studies hinted on the  
 680 existence of  $N = 6$  sub-shell closures in  $^8\text{He}$  [68] and  
 681  $^{14}\text{O}$  [69, 70]. More recently, various sides of evidence for  
 682 the  $Z = 6$  shell closure in  $^{13-20}\text{C}$  has been reported [71].  
 683 If we assume that  $N = 6$  is a robust sub-shell, the  $1/2_1^-$ ,  
 684  $3/2_1^-$  and  $5/2_1^-$  states could be viewed as composed of  
 685 one neutron in  $0p_{1/2}$  orbital outside the  $^{10}\text{Be}(0^+)$  or  
 686  $^{10}\text{Be}(2^+)$  core. The  $(2j + 1)$ -weighted energy centroid  
 687 of  $3/2_1^-$  and  $5/2_1^-$  states (shown as the dashed red line  
 688 in Fig. 5) compared to the  $1/2_1^-$  state in  $^{11}\text{Be}$ , is close  
 689 to the energy difference of the  $2_1^+$  and  $0_1^+$  states in  $^{10}\text{Be}$ .  
 690 Further, the spectroscopic factors of the  $1/2_1^-$  state and  
 691 the sum of  $3/2_1^-$  and  $5/2_1^-$  states are close to the values

692 of the  $0_1^+$  and  $2_1^+$  states for the  $^{11,12}\text{B}(d, ^3\text{He})$  transitions,  
 693 respectively (see Fig. 5). The spectroscopic study of the  
 694 negative-parity states populated in the proton removal  
 695 reactions on  $^{11,12}\text{B}$  show a consistent picture with the  
 696 valence neutron in the  $0p_{1/2}$  orbital coupling to the  $^{10}\text{Be}$   
 697 core.

## VIII. SUMMARY

698  
 699 Single-particle overlaps between negative-parity states  
 700 in  $^{11}\text{Be}$  and the ground state of  $^{12}\text{B}$  have been  
 701 determined from the measured cross sections of the  
 702  $^{12}\text{B}(d, ^3\text{He})^{11}\text{Be}$  reaction at 12 MeV/u in inverse  
 703 kinematics. Spectroscopic factors were extracted from  
 704 a DWBA analysis and compared with various theoretical  
 705 calculations from the shell model, Nilsson model and  
 706 *ab-initio* methods. Considering the dominant  $p$ -wave  
 707 neutron configuration in the  $^{12}\text{B}$  ground state, the  
 708 strong population of certain low-lying negative-parity  
 709 states in  $^{11}\text{Be}$  indicates the dominant neutron  $p$ -wave  
 710 configuration of these states.

711 Shell-model calculations using the YSOX effective  
 712 interaction reproduce the spectroscopic factors of the  
 713 low-lying negative-parity states and their excitation  
 714 energies relative to the  $1/2_1^-$  state, but the level  
 715 order of the  $5/2_1^-$  and  $3/2_1^-$  states are inverted with  
 716 respect to experiment. The VMC calculation presents  
 717 a correct level ordering although suggests far larger  
 718 mixing between excited  $3/2^-$  levels. The calculations  
 719 using the Nilsson model framework underestimate the  
 720 spectroscopic factors of  $3/2_1^-$  and  $5/2_1^-$  states. The  
 721 NCCI calculation reproduces the dominant oscillator  
 722 configurations as well as the relative excitation energies  
 723 of these states.

## ACKNOWLEDGMENTS

724  
 725 The authors would like to acknowledge the hard  
 726 work of the support and operations staff at ATLAS.  
 727 We thank John P. Schiffer and Patrick J. Fasano  
 728 for valuable discussions. This research used resources  
 729 of Argonne National Laboratory's ATLAS facility,  
 730 which is a Department of Energy Office of Science  
 731 User Facility. This material is based upon work  
 732 supported by the U.S. Department of Energy, Office  
 733 of Science, Office of Nuclear Physics, under Contract  
 734 No. DE-AC02-06CH11357 (ANL) and Grant Nos. DE-  
 735 FG02-96ER40978 (LSU), DE-FG02-95ER-40934 (ND),  
 736 DE-SC0014552 (UConn), DE-AC02-05CH11231(LBNL)  
 737 and DE-SC0009971 (CUSTIPEN). J. C. acknowledges  
 738 partial support by the FRIB-CSC Fellowship under  
 739 Grant No. 201600090345. C. X. Y. and Y. L. Y.  
 740 acknowledges the National Natural Science Foundation  
 741 of China 11775316, 11535004, 11875074. This research  
 742 used computational resources of the National Energy

743 Research Scientific Computing Center (NERSC), a 747 support from the NUCLEI SciDAC program is gratefully  
 744 U.S. Department of Energy, Office of Science, user facility 748 acknowledged. We gratefully acknowledge use of the  
 745 supported under Contract DE-AC02-05CH11231, and of 749 Bebop cluster in the Laboratory Computing Resource  
 746 the Argonne Laboratory Computing Resource Center; 750 Center at Argonne National Laboratory.

- 
- 751 [1] D. Santiago-Gonzalez, K. Auranen, M. L. Avila, A. D. 794  
 752 Ayangeakaa, B. B. Back, S. Bottoni, M. P. Carpenter, 795  
 753 J. Chen, C. M. Deibel, A. A. Hood, C. R. Hoffman, 796  
 754 R. V. F. Janssens, C. L. Jiang, B. P. Kay, S. A. 797  
 755 Kuvin, A. Lauer, J. P. Schiffer, J. Sethi, R. Talwar, 798  
 756 I. Wiedenhöver, J. Winkelbauer, and S. Zhu, Phys. Rev. 799  
 757 Lett. **120**, 122503 (2018). 800
- 758 [2] A. O. Macchiavelli *et al.*, (submitted to Phys. Rev. C). 801
- 759 [3] G.-B. Liu and H. T. Fortune, Phys. Rev. C **42**, 167 802  
 760 (1990). 803
- 761 [4] Y. Hirayama, T. Shimoda, H. Izumi, A. Hatakeyama, 804  
 762 K. Jackson, C. Levy, H. Miyatake, M. Yagi, and H. Yano, 805  
 763 Physics Letters B **611**, 239 (2005). 806
- 764 [5] D. Morrissey, K. McDonald, D. Bazin, B. Brown, 807  
 765 R. Harkewicz, N. Orr, B. Sherrill, G. Souliotis, 808  
 766 M. Steiner, J. Winger, S. Yennello, B. Young, 809  
 767 S. Lukyanov, G. Chubarian, and Y. Oganessian, Nuclear 810  
 768 Physics A **627**, 222 (1997). 811
- 769 [6] N. Aoi, K. Yoneda, H. Miyatake, H. Ogawa, Y. Ya- 812  
 770 mamamoto, E. Ideguchi, T. Kishida, T. Nakamura, M. No- 813  
 771 tani, H. Sakurai, T. Teranishi, H. Wu, S. Yamamoto, 814  
 772 Y. Watanabe, A. Yoshida, and M. Ishihara, Nuclear 815  
 773 Physics A **616**, 181 (1997), radioactive Nuclear Beams. 816
- 774 [7] H. Bohlen, R. Kalpakchieva, W. von Oertzen, T. Massey, 817  
 775 B. Gebauer, S. Grimes, T. Kokalova, H. Lenske, A. Lenz, 818  
 776 M. Milin, C. Schulz, S. Thummerer, S. Torilov, and 819  
 777 A. Tumino, Nuclear Physics A **722**, C3 (2003). 820
- 778 [8] H. G. Bohlen, W. von Oertzen, R. Kalpakchieva, T. N. 821  
 779 Massey, T. Dorsch, M. Milin, C. Schulz, T. Kokalova, 822  
 780 and C. Wheldon, Journal of Physics: Conference Series 823  
 781 **111**, 012021 (2008). 824
- 782 [9] H. T. Fortune and R. Sherr, Phys. Rev. C **83**, 054314 825  
 783 (2011). 826
- 784 [10] H. T. Fortune, Phys. Rev. C **86**, 037302 (2012). 827
- 785 [11] G. Mairle and G. Wagner, Nuclear Physics A **253**, 253 828  
 786 (1975). 829
- 787 [12] J. Lind, G. Garvey, and R. Tribble, Nuclear Physics A 830  
 788 **276**, 25 (1977). 831
- 789 [13] H. Y. Lee, J. P. Greene, C. L. Jiang, R. C. Pardo, K. E. 832  
 790 Rehm, J. P. Schiffer, A. H. Wuosmaa, N. J. Goodman, 833  
 791 J. C. Lighthall, S. T. Marley, K. Otsuki, N. Patel, 834  
 792 M. Beard, M. Notani, and X. D. Tang, Phys. Rev. C 835  
 793 **81**, 015802 (2010). 836
- [14] A. Wuosmaa, J. Schiffer, B. Back, C. Lister, and 837  
 K. Rehm, Nucl. Instr. Meth. Phys. Res. Sect. A **580**, 838  
 1290 (2007). 839
- [15] J. Lighthall, B. Back, S. Baker, S. Freeman, H. Lee, 840  
 B. Kay, S. Marley, K. Rehm, J. Rohrer, J. Schiffer, 841  
 D. Shetty, A. Vann, J. Winkelbauer, and A. Wuosmaa, 842  
 Nucl. Instr. Meth. Phys. Res. Sec. A **622**, 97 (2010). 843
- [16] S. Bedoor, A. H. Wuosmaa, M. Albers, M. Alcorta, 844  
 S. Almaraz-Calderon, B. B. Back, P. F. Bertone, C. M. 845  
 Deibel, C. R. Hoffman, J. C. Lighthall, S. T. Marley, 846  
 D. G. Mcneel, R. C. Pardo, K. E. Rehm, J. P. Schiffer, 847  
 and D. V. Shetty, Phys. Rev. C **93**, 044323 (2016). 848
- [17] J. Kelley, E. Kwan, J. Purcell, C. Sheu, and H. Weller, 849  
 Nuclear Physics A **880**, 88 (2012). 850
- [18] N. Fukuda, T. Nakamura, N. Aoi, N. Imai, M. Ishihara, 851  
 T. Kobayashi, H. Iwasaki, T. Kubo, A. Mengoni, 852  
 M. Notani, H. Otsu, H. Sakurai, S. Shimoura, 853  
 T. Teranishi, Y. X. Watanabe, and K. Yoneda, Phys. 854  
 Rev. C **70**, 054606 (2004). 855
- [19] C. R. Hoffman, B. B. Back, B. P. Kay, J. P. Schiffer, 856  
 M. Alcorta, S. I. Baker, S. Bedoor, P. F. Bertone, J. A. 857  
 Clark, C. M. Deibel, B. DiGiovine, S. J. Freeman, J. P. 858  
 Greene, J. C. Lighthall, S. T. Marley, R. C. Pardo, K. E. 859  
 Rehm, A. Rojas, D. Santiago-Gonzalez, D. K. Sharp, 860  
 D. V. Shetty, J. S. Thomas, I. Wiedenhöver, and A. H. 861  
 Wuosmaa, Phys. Rev. C **85**, 054318 (2012). 862
- [20] M. H. Macfarlane and S. C. Pieper, *Report ANL-76-11*, 863  
*Rev. 1, 1978 (unpublished)*, . 864
- [21] H. An and C. Cai, Phys. Rev. C **73**, 054605 (2006). 865
- [22] D. Y. Pang, P. Roussel-Chomaz, H. Savajols, R. L. 866  
 Varner, and R. Wolski, Phys. Rev. C **79**, 024615 (2009). 867
- [23] R. B. Wiringa, V. G. J. Stoks, and R. Schiavilla, Phys. 868  
 Rev. C **51**, 38 (1995). 869
- [24] Y. Han, Y. Shi, and Q. Shen, Phys. Rev. C **74**, 044615 870  
 (2006). 871
- [25] W. W. Daehnick, J. D. Childs, and Z. Vrcelj, Phys. Rev. 872  
 C **21**, 2253 (1980). 873
- [26] R. Varner, W. Thompson, T. McAbee, E. Ludwig, and 874  
 T. Clegg, Phys. Rep. **201**, 57 (1991). 875
- [27] J. Lohr and W. Haeberli, Nuclear Physics A **232**, 381 876  
 (1974). 877
- [28] C.-T. Liang, X.-H. Li, and C.-H. Cai, Journal of Physics 878  
 G: Nuclear and Particle Physics **36**, 085104 (2009). 879

- [29] M. H. Macfarlane and J. B. French, *Rev. Mod. Phys.* **32**, 567 (1960).
- [30] U. Schwinn, G. Mairle, G. J. Wagner, and C. Ramer, *Zeitschrift fur Physik A Atoms and Nuclei* **275**, 241 (1975).
- [31] G. Mairle, L. K. Pao, G. J. Wagner, K. T. Knopfle, and H. Riedesel, *Zeitschrift fur Physik A Atoms and Nuclei* **301**, 157 (1981).
- [32] D. Scott, P. Portner, J. Nelson, A. Shotter, A. Mitchell, N. Chant, D. Montague, and K. Ramavataram, *Nuclear Physics A* **141**, 497 (1970).
- [33] K. T. Schmitt, K. L. Jones, A. Bey, S. H. Ahn, D. W. Bardayan, J. C. Blackmon, S. M. Brown, K. Y. Chae, K. A. Chipps, J. A. Cizewski, K. I. Hahn, J. J. Kolata, R. L. Kozub, J. F. Liang, C. Matei, M. Matoš, D. Matyas, B. Moazen, C. Nesaraja, F. M. Nunes, P. D. O'Malley, S. D. Pain, W. A. Peters, S. T. Pittman, A. Roberts, D. Shapira, J. F. Shriner, M. S. Smith, I. Spassova, D. W. Stracener, A. N. Villano, and G. L. Wilson, *Phys. Rev. Lett.* **108**, 192701 (2012).
- [34] C. Yuan, T. Suzuki, T. Otsuka, F. Xu, and N. Tsunoda, *Phys. Rev. C* **85**, 064324 (2012).
- [35] A. O. Macchiavelli, H. L. Crawford, C. M. Campbell, R. M. Clark, M. Cromaz, P. Fallon, M. D. Jones, I. Y. Lee, and M. Salathe, *Phys. Rev. C* **97**, 011302 (2018).
- [36] B. A. Brown, A. Etchegoyen, N. S. Godwin, W. Rae, W. D.M. Richter, W. Ormand, E. Warburton, J. Winfield, L. Zhao, and C. H. Zimmerman, (Oxbash for Windows, Report MSU NSCL report number 1289).
- [37] E. K. Warburton and B. A. Brown, *Phys. Rev. C* **46**, 923 (1992).
- [38] W. von Oertzen, M. Freer, and Y. Kanada-En'yo, *Physics Reports* **432**, 43 (2006).
- [39] V. M. Datar, S. Kumar, D. R. Chakrabarty, V. Nanal, E. T. Mirgule, A. Mitra, and H. H. Oza, *Phys. Rev. Lett.* **94**, 122502 (2005).
- [40] A. Bohr and B. R. Mottelson, *R 1998 Nuclear Structure, vol. II, p. 33, World Scientific, Singapore, .*
- [41] P. Navratil, J. P. Vary, and B. R. Barrett, *Phys. Rev. Lett.* **84**, 5728 (2000).
- [42] T. Neff and H. Feldmeier, *Nucl. Phys. A* **738**, 357 (2004).
- [43] G. Hagen, D. J. Dean, M. Hjorth-Jensen, T. Papenbrock, and A. Schwenk, *Phys. Rev. C* **76**, 044305 (2007).
- [44] S. Quaglioni and P. Navratil, *Phys. Rev. C* **79**, 044606 (2009).
- [45] S. Bacca, N. Barnea, and A. Schwenk, *Phys. Rev. C* **86**, 034321 (2012).
- [46] N. Shimizu, T. Abe, Y. Tsunoda, Y. Utsuno, T. Yoshida, T. Mizusaki, M. Honma, and T. Otsuka, *Prog. Exp. Theor. Phys.* **2012**, 01A205 (2012).
- [47] T. Dytrych, K. D. Launey, J. P. Draayer, P. Maris, J. P. Vary, E. Saule, U. Catalyurek, M. Sosonkina, D. Langr, and M. A. Caprio, *Phys. Rev. Lett.* **111**, 252501 (2013).
- [48] B. R. Barrett, P. Navratil, and J. P. Vary, *Prog. Part. Nucl. Phys.* **69**, 131 (2013).
- [49] S. Baroni, P. Navratil, and S. Quaglioni, *Phys. Rev. C* **87**, 034326 (2013).
- [50] J. Carlson, S. Gandolfi, F. Pederiva, S. C. Pieper, R. Schiavilla, K. E. Schmidt, and R. B. Wiringa, *Rev. Mod. Phys.* **87**, 1067 (2015).
- [51] D. R. Entem and R. Machleidt, *Phys. Rev. C* **68**, 041001 (2003).
- [52] E. Epelbaum, H.-W. Hammer, and U.-G. Meißner, *Rev. Mod. Phys.* **81**, 1773 (2009).
- [53] I. Brida, S. C. Pieper, and R. B. Wiringa, *Phys. Rev. C* **84**, 024319 (2011).
- [54] A. M. Shirokov, I. J. Shin, Y. Kim, M. Sosonkina, P. Maris, and J. P. Vary, *Phys. Lett. B* **761**, 87 (2016).
- [55] M. A. Caprio, P. J. Fasano, J. P. Vary, P. Maris, and J. Hartley, in *Proceedings of the International Conference Nuclear Theory in the Supercomputing Era 2018*, edited by A. M. Shirokov and A. I. Mazur (Pacific National University, Khabarovsk, Russia, in press) arXiv:1909.13417.
- [56] P. Maris, M. Sosonkina, J. P. Vary, E. Ng, and C. Yang, *Procedia Comput. Sci.* **1**, 97 (2010).
- [57] H. M. Aktulga, C. Yang, E. G. Ng, P. Maris, and J. P. Vary, *Concurrency Computat.: Pract. Exper.* **26**, 2631 (2013).
- [58] M. Shao, H. M. Aktulga, C. Yang, E. G. Ng, P. Maris, and J. P. Vary, *Comput. Phys. Commun.* **222**, 1 (2018).
- [59] S. K. Bogner, R. J. Furnstahl, P. Maris, R. J. Perry, A. Schwenk, and J. Vary, *Nucl. Phys. A* **801**, 21 (2008).
- [60] P. Maris, J. P. Vary, and A. M. Shirokov, *Phys. Rev. C* **79**, 014308 (2009).
- [61] P. Maris and J. P. Vary, *Int. J. Mod. Phys. E* **22**, 1330016 (2013).
- [62] S. L. Henderson, T. Ahn, M. A. Caprio, P. J. Fasano, A. Simon, W. Tan, P. O'Malley, J. Allen, D. W. Bardayan, D. Blankstein, B. Frenzt, M. R. Hall, J. J. Kolata, A. E. McCoy, S. Moylan, C. S. Reingold, S. Y. Strauss, and R. O. Torres-Isea, *Phys. Rev. C* **99**, 064320 (2019).
- [63] P. Maris, M. A. Caprio, and J. P. Vary, *Phys. Rev. C* **91**, 014310 (2015); **99**, 029902(E) (2019).
- [64] M. A. Caprio, P. Maris, J. P. Vary, and R. Smith, *Int. J. Mod. Phys. E* **24**, 1541002 (2015).
- [65] M. A. Caprio *et al.*, (in preparation).

- 935 [66] A. M. Shirokov, I. J. Shin, Y. Kim, M. Sosonkina, 948  
 936 P. Maris, and J. P. Vary, in *Book of Abstracts of the* 949  
 937 *XXII International Conference on Few-Body Problems in* 950  
 938 *Physics (FB22)* (2018). 951
- 939 [67] Y. Kim, I. J. Shin, A. M. Shirokov, M. Sosonkina, 952 [69] I. Angeli and K. Marinova, *Atomic Data and Nuclear*  
 940 P. Maris, and J. P. Vary, in *Proceedings of the Interna-* 953 *Data Tables* **99**, 69 (2013).  
 941 *tional Conference Nuclear Theory in the Supercomputing* 954 [70] T. Otsuka, R. Fujimoto, Y. Utsuno, B. A. Brown,  
 942 *Era 2018*, edited by A. M. Shirokov and A. I. Mazur 955 M. Honma, and T. Mizusaki, *Phys. Rev. Lett.* **87**, 082502  
 943 (Pacific National University, Khabarovsk, Russia, in 956 (2001).  
 944 press) arXiv:1910.04367. 957 [71] D. Tran, H. Ong, and et al., *Nature Communications* **9**,  
 945 [68] F. Skaza, V. Lapoux, N. Keeley, N. Alamanos, E. C. 958 1 (2018).  
 946 Pollacco, F. Auger, A. Drouart, A. Gillibert, D. Beaumel,  
 947 E. Becheva, Y. Blumenfeld, F. Delaunay, L. Giot,